Nonlinear properties of quantum dot semiconductor optical amplifiers at 1.3 μm

Invited Paper

D. Bimberg[1], C. Meuer[1], M. Lämmlin[1], S. Liebich[1], J. Kim[1], A. Kovsh[2], I. Krestnikov[2], and G. Eisenstein[1,3]

[1]*Institut für Festkörperphysik, Technische Universität Berlin, EW 5-2, Hardenbergstr. 36, 10623 Berlin, Germany*

[2]*Innolume GmbH, Konrad-Adenauer-Allee 11, 40263 Dortmund, Germany*

[3]*Electrical Engineering Department, Technion, Haifa 32000, Israel*

Received May 16, 2008

The dynamics of nonlinear processes in quantum dot (QD) semiconductor optical amplifiers (SOAs) are investigated. Using small-signal measurements, the suitabilities of cross-gain and cross-phase modulation as well as four wave mixing (FWM) for wavelength conversion are examined. The cross-gain modulation is found to be suitable for wavelength conversion up to a frequency of 40 GHz.

OCIS codes: 250.5980, 250.5590, 190.4720.

doi: 10.3788/COL20080610.0724.

Quantum dot (QD) semiconductor optical amplifiers (SOAs) being low cost and high performance are of largest importance for future all optical networks like 100-Gb/s Ethernet using the O-band (1260 − 1360 nm)[1,2]. In these optical networks, SOAs will be used as linear amplifiers for the compensation of splitting losses as well as for wavelength conversion, switching and regeneration which are based on nonlinear effects occurring when the SOA is driven into saturation. The most important of the latter ones are cross-gain modulation (XGM), cross-phase modulation (XPM) and four wave mixing (FWM). QD SOAs benefit from several unique features arising from the particular electronic structure of the QDs. Due to the inhomogeneous size distribution of the QDs, the gain bandwidth is inhomogeneously broadened and large[3]. Gain recovery dynamics within the QD has been shown to be ultrafast (130 fs). The fast dynamics enable pattern-effect free amplification of 40-Gb/s data streams and above[4] demonstrated until now for 1.5-μm[5] QD SOAs and allow for high speed wavelength conversion using XGM at 40 Gb/s as shown here. Within this paper the dynamical properties of XGM and XPM as well as FWM are investigated using small-signal measurements at 1.3 μm. XGM is found to be suitable for wavelength conversion up to a frequency of 40 GHz.

The InAs QDs are stacked 10 fold in a GaAs core, placed between AlGaAs cladding layers, grown by molecular beam epitaxy. The dots are covered by a 5-nm-thick $In_{0.15}Ga_{0.85}As$ quantum well (QW) layer to extend the emission wavelength to 1.3 μm[6]. A 33-nm-thick GaAs p-doped spacer separating the QD layers ensures strain relaxation and thus minimization of defects in the 10 stacks of QDs. Luminescence experiments display the QD ground state (GS) which is used for amplification and excited states (ESs). These and the higher energy levels in the QWs act as a carrier reservoir which refills the QD states after depletion. The time constants for carrier relaxation between and within these levels range from 130 fs for the ES to GS[7] relaxation to several hundred picoseconds for complete gain recovery and relaxation to thermal equilibrium within the QW carrier distribution after depletion[8].

Ridge waveguide structures of 4-μm width were cleaved to 2-mm-long SOAs. The ridge was dry etched through the active core layer containing the QDs to provide strong index guiding of the optical mode and to suppress current spreading[9]. The waveguide end facets were tilted at 6.8° and were anti-reflection coated.

The characterization setup included tapered fibers for coupling in and out of the SOA waveguide. The measured coupling loss per facet was 4 dB. The maximum linear chip gain and saturation output power were 19 dB and +14 dBm, respectively. This corresponds to a chip saturation input power of −2 dBm. The residual gain ripple was smaller than 2 dB.

The small-signal XGM experiments[10] were performed using a HP 8722C network analyzer. A saturating pump signal from a 1311-nm distributed feedback (DFB) laser diode is externally modulated by a small sinusoidal signal. The pump is injected into the QD SOA together with a non-saturating continuous wave (CW) probe signal from a wavelength tunable external cavity laser (ECL). The ECL signal probes the gain spectrum and experiences the modulation via XGM. The pump is filtered at the SOA output using a fiber Bragg grating and a tunable filter. The probe is detected and its modulation characteristics are analyzed by the network analyzer. The electrical S_{21} parameter is transformed to units of optical power and normalized to the response of the pump without the QD SOA, called XGM efficiency.

The setup for measuring FWM is similar to the XGM setup except that the power levels of the pump and probe signals are comparable. The probe signal is modulated whereas the pump is a CW signal. After the QD SOA, the filters are tuned to the wavelength of the FWM signal in order to analyze it by the network analyzer.

In the XPM setup the QD SOA is inserted into a sagnac interferometer. The pump signal is modulated using a sine generator (E8247C, Agilent, USA) and the

CW probe signal is analyzed by an electrical spectrum analyzer (FSU 50, Rohde & Schwarz, Germany). For each modulation frequency, the output of the CW signal at the destructive port is minimized using a variable optical delay line. A filter at the destructive output is used to block the pump signal. The XPM efficiency is determined by comparing the electrical power of the modulation line at the input of the loop to the value measured at the output, given in units of optical power. The XPM measurements suffered from noise caused by polarization mode beating due to the fact that the QD SOAs are not polarization insensitive. This results in an error margin of about 1 dB.

XGM is shown for different bias currents in Fig. 1. Two regimes can be identified. The first is a decrease of the efficiency from 50 MHz up to around 10 GHz. For higher frequencies from 10 up to 40 GHz the efficiency is almost frequency independent. We attribute the decrease at low frequencies to the dynamics of the carrier reservoir in the QW which has a recovery time around 100 ps, as can be seen from pump-probe measurements[8]. Thus the recovery upon carrier depletion in the reservoir is comparatively slow. Above 10 GHz the reservoir cannot respond to the modulation and is fixed at an average value. The QDs themselves show ultrafast gain recovery after spectral hole burning and can follow the modulation even at higher frequencies which explains the flat trend up to 40 GHz. By increasing the current, the saturation of the reservoir is reduced, and as a consequence the dynamics of the QDs is improved. Thus, the 3-dB bandwidth of the XGM can be tuned from 10 GHz for lowest current, i.e., dominating reservoir dynamics, to bandwidths beyond 40 GHz under optimum conditions, i.e., high bias current and dominating QD dynamics. The present XGM efficiency of −8 dB could be increased to larger values with devices which show higher gain.

The difference between the two regimes is also visible in the wavelength-dependent measurements depicted in Fig. 2. The pump is set to 1311 nm while the detuning between pump and probe is varied. In order to eliminate the influence of the gain spectrum, the XGM traces are normalized to their respective maxima and several frequencies are picked. Therefore, at frequencies below 3 GHz the XGM response appears as a flat line, whereas at 10 GHz and above, a wavelength dependence is observed. Again this can be explained by the reservoir dynamics which couples the whole QD gain spectrum at lower frequencies. At 10 GHz and above, the reservoir cannot respond, and a mixture of total carrier depletion

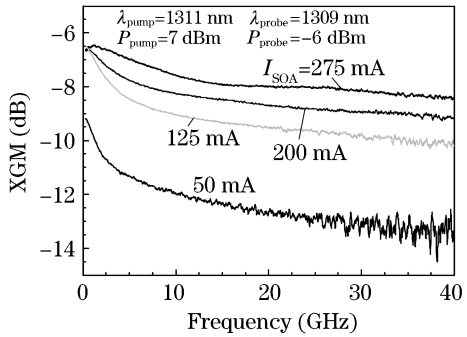

Fig. 1. XGM efficiency and frequency dependence for various drive currents.

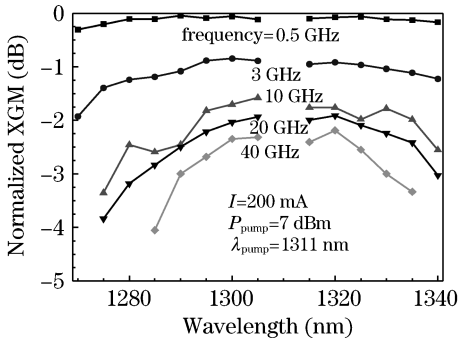

Fig. 2. Normalized XGM changing with detuning for different frequencies.

and spectral hole burning which only affects QDs within the homogeneous linewidth is seen.

The XPM is mainly governed by the dynamics of the carrier reservoir in the QW and bulk material as described in Ref. [11]. The decoupling of the gain of the QDs themselves and the phase dominated by the reservoir dynamics are promising to show XPM without simultaneous XGM using an interferometer setup. However, as seen in the XGM measurements, the XPM is expected to be limited to bandwidths below 10 GHz as a consequence of the slow dynamics reservoir. Similar to XGM, increased current and higher input power lead to an enhanced efficiency shown in Fig. 3. Frequency-dependent measurements and wavelength detuning revealed the limitation of the 3-dB XPM bandwidth to 10 GHz already predicted above (Fig. 4). In contrast to the XGM, XPM shows no wavelength dependence, which is reasonable because the reservoir depletion affects all

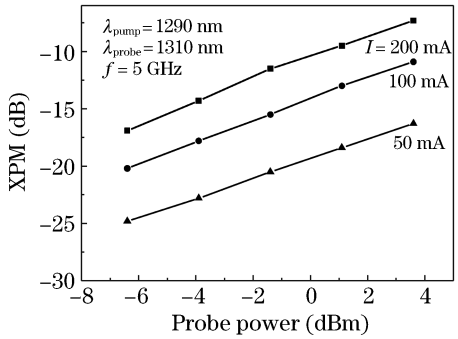

Fig. 3. XPM for different currents dependent on the probe power.

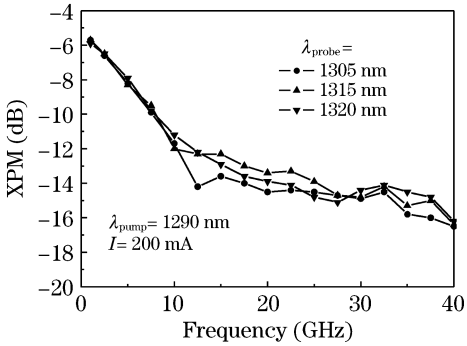

Fig. 4. Wavelength scan of XPM frequency response.

QDs. This demonstrates that XPM is hardly applicable for wavelength conversion, if the reservoir dynamics is not enhanced. On the other hand, switching using short pulses or switching of long data bursts might be possible.

The static characterization of the FWM conversion efficiency is depicted in Fig. 5. A minimum detuning of 1.7 nm is assumed, to enable suppression of the pump and probe and to analyze the FWM signal. The dependence of the conversion efficiency on the detuning is comparable to values given in the literature within a margin of 10 to 15 dB. A slight asymmetry of the conversion efficiency between positive and negative detuning is caused by the Bogatov effect[12]. The low conversion efficiency and the small signal-to-noise ratio make it difficult to use FWM for wavelength conversion unless the nonlinearity is increased, e.g., by optimization of the waveguide geometry. The frequency response of FWM shows a flat dependence within up to 40 GHz reflecting the ultrafast dynamics of the QDs (Fig. 6). The strong dependence of spectral hole burning on the detuning causes a decreasing efficiency above 20 GHz for detuning of 3.7 nm and more.

We have investigated nonlinear effects in QD SOAs, including XGM and XPM as well as FWM, using small-signal modulation. Two different saturation mechanisms contribute to the nonlinearity observed, total carrier depletion of the reservoir in higher energy QW states resulting in a bandwidth of 10 GHz and spectral hole burning which exhibits bandwidths beyond 40 GHz, within a spectral range defined by the homogeneous linewidth. The nonlinear efficiency and the cut-off frequency bandwidth increase for increased bias current and pump power, because the saturation of the reservoir is reduced. For wavelength conversion XGM is the most suitable. Under optimum operating conditions bandwidths above 40 GHz are measured. However, data signal measurements should be conducted to judge the influence of patterning on the wavelength conversion possibly occurring due to the slow reservoir dynamics. FWM and XPM suffer from low efficiency and limited bandwidth, respectively. Due to the decoupling of gain and phase[11], XPM is well suited for packet switching and switching of short pulses.

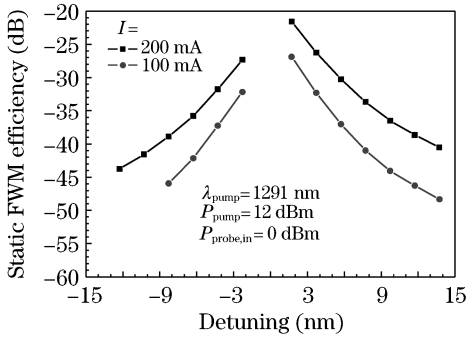

Fig. 5. Static FWM conversion efficiency at currents of 100 and 200 mA.

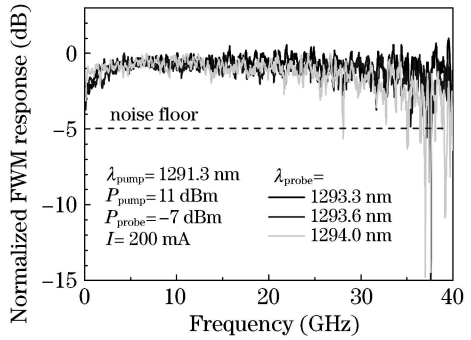

Fig. 6. Dynamical FWM response for several detunings.

This work was supported by the SANDiE NoE of the European Commission (No. NMP4-CT-2004-500101), the TRIUMPH Project IST-027638 STP, the State of Berlin (ProFIT MonoPic and OptiDot), and the Sonderforschungsbereich SFB 787 of the German Research Council. G. Eisenstein is a Humboldt awardee at TU Berlin and thanks the Humboldt foundation for its support. D. Bimberg's e-mail address is Bimberg@physik.tu-berlin.de.

References

1. D. Bimberg, Electron. Lett. **44,** 390 (2008).
2. D. Bimberg, M. Kuntz, and M. Laemmlin, Appl. Phys. A **80,** 1179 (2005).
3. D. Bimberg, N. Kirstaedter, N. N. Ledentsov, Zh. I. Alferov, P. S. Kop'ev, and V. M. Ustinov, IEEE J. Sel. Top. Quantum Eelectron. **3,** 197 (1997).
4. S. Dommers, V. V. Temnov, U. Woggon, J. Gomis, J. Martinez-Pastor, M. Laemmlin, and D. Bimberg, Appl. Phys. Lett. **90,** 033508 (2007).
5. T. Akiyama, M. Ekawa, M. Sugawara, K. Kawaguchi, H. Sudo, A. Kuramata, H. Ebe, and Y. Arakawa, IEEE Photon. Technol. Lett. **17,** 1614 (2005).
6. A. R. Kovsh, N. A. Maleev, A. E. Zhukov, S. S. Mikhrin, A. P. Vasil'ev, E. A. Semenova, Yu. M. Shernyakov, M. V. Maximov, D. A. Livshits, V. M. Ustinov, N. N. Ledentsov, D. Bimberg, and Zh. I. Alferov, J. Cryst. Growth **251,** 729 (2003).
7. P. Borri, W. Langbein, J. M. Hvam, F. Heinrichsdorff, H.-M. Mao, and D. Bimberg, IEEE J. Sel. Top. Quantum Electron. **6,** 544 (2000).
8. T. Vallaitis, C. Koos, R. Bonk, W. Freude, M. Laemmlin, C. Meuer, D. Bimberg, and J. Leuthold, Opt. Express **16,** 170 (2008).
9. D. Ouyang, N. N. Ledentsov, D. Bimberg, A. R. Kovsh, A. E. Zhukov, S. S. Mikhrin, and V. M. Ustinov, Semicond. Sci. Technol. **18,** L53 (2003).
10. R. Alizon, A. Bilenca, H. Dery, V. Mikhelashvili, G. Eisenstein, R. Schwertberger, D. Gold, J. P. Reithmaier, and A. Forchel, Appl. Phys. Lett. **82,** 4660 (2003).
11. A. V. Uskov, E. P. O'Reilly, R. J. Manning, R. P. Webb, D. Cotter, M. Laemmlin, N. N. Ledentsov, and D. Bimberg, IEEE Photon. Technol. Lett. **16,** 1265 (2004).
12. A. P. Bogatov, P. G. Eliseev, and B. N. Sverdlov, IEEE J. Quantum Electron. **11,** 510 (1975).